AD_____

AWARD NUMBER: DAMD17-03-1-0584

TITLE: Trafficking of Metastatic Breast Cancer Cells in Bone

PRINCIPAL INVESTIGATOR: Andrea M. Mastro, Ph.D.

CONTRACTING ORGANIZATION: Pennsylvania State University
University Park, Pennsylvania 16802-7000

REPORT DATE: August 2006

TYPE OF REPORT: Final

PREPARED FOR: U.S. Army Medical Research and Materiel Command
Fort Detrick, Maryland 21702-5012

REPORT DOCUMENTATION PAGE

Form Approved
OMB No. 0704-0188

1. REPORT DATE *(DD-MM-YYYY)*	**2. REPORT TYPE**	**3. DATES COVERED** *(From - To)*
01-08-2006	Final	1 Aug 2003 – 31 Jul 2006

4. TITLE AND SUBTITLE

Trafficking of Metastatic Breast Cancer Cells in Bone

5a. CONTRACT NUMBER

5b. GRANT NUMBER
DAMD17-03-1-0584

5c. PROGRAM ELEMENT NUMBER

6. AUTHOR(S)

Andrea M. Mastro, Ph.D.

E-Mail: a36@psu.edu

5d. PROJECT NUMBER

5e. TASK NUMBER

5f. WORK UNIT NUMBER

7. PERFORMING ORGANIZATION NAME(S) AND ADDRESS(ES)

Pennsylvania State University
University Park, Pennsylvania 16802-7000

8. PERFORMING ORGANIZATION REPORT NUMBER

9. SPONSORING / MONITORING AGENCY NAME(S) AND ADDRESS(ES)
U.S. Army Medical Research and Materiel Command
Fort Detrick, Maryland 21702-5012

10. SPONSOR/MONITOR'S ACRONYM(S)

11. SPONSOR/MONITOR'S REPORT NUMBER(S)

12. DISTRIBUTION / AVAILABILITY STATEMENT
Approved for Public Release; Distribution Unlimited

13. SUPPLEMENTARY NOTES

14. ABSTRACT

Breast cancer metastases are usually found at the ends (metasphyses) of long bones where they cause osteolysis. The objective was to determine the trafficking of cancer cells in the marrow cavity and to identify factors that attract them. Human breast cancer cells that express green fluorescent protein (MDA-MB 231GFP) were inoculated intracardiacly into athymic mice.; femurs harvested from 1 hr to 6 wk later and analyzed by fluorescence microscopy, immunohistochemistry, histomorphometry, flow cytometry and PCR. Single cells were detected within 1 hr in the distal metasphyses. Most cleared the marrow by 72 hr; but at 1 wk small foci formed in the ends near osteoblasts. At 2 wk the foci grew and coalesced. By 4 wk, the tumor masses were large and extended into the diaphysis. The osteoblasts were dramatically reduced (8% of control), while osteoclasts were reduced modestly (~60% of control). Ours is the first in vivo evidence that tumor cells influence not only osteoclasts, as widely believed, but also eliminate functional osteoblasts, thereby restructuring the bone microenvironment to strongly favor osteolysis. Using an ELISA array we also found that the metasphyseal bone was rich in several cyokines and factors that were only weakly detected in the shaft of the bone. Strategies that restore osteoblast function, perhaps by modifying the bone microenvironment, are needed to improve treatment of osteolytic bone metastases.

15. SUBJECT TERMS
breast cancer, bone, metastasis, trafficking

16. SECURITY CLASSIFICATION OF:			**17. LIMITATION OF ABSTRACT**	**18. NUMBER OF PAGES**	**19a. NAME OF RESPONSIBLE PERSON**
a. REPORT	**b. ABSTRACT**	**c. THIS PAGE**			USAMRMC
U	U	U	UU	27	**19b. TELEPHONE NUMBER** *(include area code)*

Table of Contents

Cover……1

SF 298……2

Introduction……4

Body……4-12

Key Research Accomplishments……13

Reportable Outcomes……13-15

Conclusions……15

References……16-17

Appendices……18

Phadke et al. Kinetics of Metastatic Breast Cancer Cell Trafficking in Bone, Clin Cancer Research
12: 1431, 2006.

INTRODUCTION

Breast cancer cells frequently metastasize to bone where they cause osteolytic lesions. The bone loss is associated with fractures, bone pain and hypercalcemia and is a major medical problem (Body 1992, Coleman 1997). At the time of death, metastatic bone disease accounts for the bulk of the tumor burden (Mundy 2002). The tumor masses and the osteolytic lesions are usually found at the ends of long bones, i.e. the metaphyses. However, the basic biology of this event is not understood (Mundy 2002). For example, it is not known how breast cancer cells arrive at their destination and what attracts them to this site. The objective of this study was to determine the trafficking patterns of breast cancer cells early upon their arrival in the bone marrow cavity and to identify factors that attract the cells to the metaphyseal ends of the bone. The development of green fluorescent protein (GFP)-expressing breast cancer cells allowed us to detect metastases prior to bone loss (Harms et al. 2002). Athymic mice were inoculated with human metastatic breast cancer cells engineered to express GFP, i.e. MDA-MB-435 ($MDA435^{GFP}$) by intracardiac injection and the femurs harvested at various times from 1 hr to 6 wk. Some femurs were fixed and decalcified for immunohistochemistry and histomorphometry in order to detect the presence of the cancer cells and the state of the osteoblasts and osteoclasts. From other femurs, the marrow was collected from the distal, proximal metaphyses and from the shaft (diaphysis) of the bone marrow cavity. The cells from the marrow cavity were analyzed by flow cytometry for GFP positive cells and with quantitative real-time PCR for a human gene, HERVK. In addition marrow and bone from the metaphyses and diaphyses were incubated for 24 hr. The culture preparations were screened for the presence of cytokines and growth factors (Muller et al. 2001).

BODY

Task 1: To determine how metastatic breast cancer cells partition among the metaphyseal, endosteal, and cortical bone marrows.

The first task was to determine how metastatic breast cancer cells partition between the metaphysis and diaphysis; and, in the diaphysis, if they tended to be next to the bone (endosteal) or in the more central (cortical) bone marrow in the femurs from mice inoculated with $MDA435^{GFP}$ breast cancer cells. We extended the study to examine separately the proximal

(hip) metaphyseal region versus the distal (knee) metaphyseal regions of the femur.

We have carried out several major experiments, some with a collaborator, Dr. Danny Welch, University of Alabama-Birmingham. Together we have published a manuscript (see Phadke et al. 2006, appendix) summarizing the results of this work. The data in the appended manuscript are referred to in this text.

Athymic mice were inoculated by intracardiac injection (approximately $3x10^5$ breast cancer cells). At various times, (1 hr, 2 hr, 4 hr, 8 hr, 24 hr, 72 hr, 1 week, 2 weeks, 4 weeks, 6 weeks) the femurs were harvested. Upon removal from the animal, the intact femurs were inspected with a fluorescent stereomicroscope. Tumor cells could be seen in the bone (Figure 1, below and Figure 1, Phadke et al 2006). They were first noted in the distal ends of the femur (Figure 1 below).

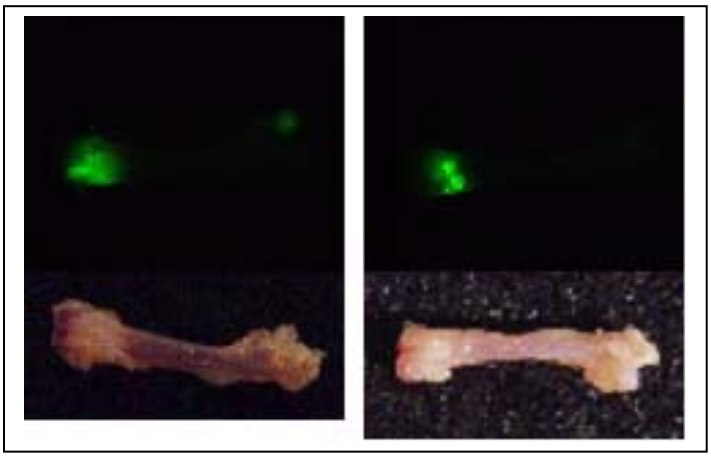

Figure 1. Femurs were removed from mice 4wk following inoculation with MB-435^{GFP} cells and visualized by bright field (bottom) and fluorescent microscopy.

The remaining figures can be found in the appended publication by Phadke et al. Clinical Cancer Research 12: 1431-1440, 2006 (reference 1).

Numerous solitary cells were seen after 1 hr of injection, (Figure 1 Phadke et al.), and fluorescent foci were seen by 1 week. These coalesced into larger foci (Figure 1, A2-A3) and tumor masses sometimes filled the entire marrow cavity (4-6 weeks Figure 1F,G). Early after

inoculation, tumor cells were more readily seen in the metaphysis before they could be seen in the diaphysis (Figure 2, Phadke et al.).

Sections of fixed and decalcified bone were examined by anti-GFP immunohistochemistry (Figure 1B, Phadke et al.) or examined directly by fluorescence confocal microscopy (Figure 1E Phadke et al). We detected approximately the same numbers of cells using both techniques. It was difficult to find single cells in individual sections of femurs taken from mice before about 1 wk post inoculation (note individual cell in Figure 1 B1, Phadke et al). However, at later times the MDA-435^{GFP} cells were easily detected (Figure 1 B2-4, E1-3 Phadke et al). Masses of tumor cells were seen in the marrow cavity by 4-6 weeks (Figure 1 F, G, Phadke et al.). A comparison of the trabecular bone in femurs with a cancer mass (Figure 1D, Phadke et al) was significantly less than that seen in bones from normal animals (Figure 1C, Phadke et al.) indicating osteolytic degradation.

Both flow cytometry and real time PCR (RT-PCR) were used to quantitate the numbers of cancer cells in the femur (Figure 2, Phadke et al). We estimated that only a small fraction (0.01%) of the injected cells could be found in a femur (Table 1, Phadke et al). These procedures also indicated that the pattern of distribution of the cancer cells was similar to that seen with the histological approaches. It should be pointed out that localization is not as precise with these techniques because cutting the metaphysis from the diaphysis was not absolutely accurate. We also found that the tumor cells in the diaphysis were largely (>95%) near the endosteal bone and not in the central marrow (Figure 5G Phadke et al). This pattern is similar to that seen with the distribution of hematopoietic cells in the bone marrow (Mason et al. 1989).

We had previously found with *in vitro* co-culture that breast cancer cells caused an increase in osteoblast apoptosis and that the osteoblasts did not differentiate into bone matrix forming cells (Mastro et al. 2004; Mercer et al. 2004; Mercer and Mastro 2005). Therefore, we carried out histochemical analyses to determine if the cancer cells affected the osteoblasts the same way *in vivo*. Using a fluoresent TUNEL assay, we saw that apoptotic osteoblasts increased in femurs following the inoculation of the cancer cells (Figure 3D,G Phadke et al). We also noted that apoptotic osteoblasts tended to be within 50 microns of a cancer cell (Figure 4 Phadke et al.).

Staining of cryosections of femur for bone alkaline phosphatase activity to assess the level of the maturity of the osteoblasts, revealed that the trabecular bone from the cancer bearing animals had very little alkaline phosphatase activity compared to control bones (Figure 3 H,I, Phadke et al.). The alkaline phosphatase activity in the growth plates of the bone was similar, however. These data together indicated that in the cancer bearing bone, the osteoblasts in the trabecular bone were undergoing apoptosis and also were unable to differentiate. Histomorphometry confirmed that there were significantly fewer osteoblasts in bone of cancer bearing mice (Figure 3B, Phadke et al). A comparison of the ratios of calcified bone volume/tissue volume indicated that calcified bone was significantly lost by 4 weeks (Figure 3A, Phadke et al.).

We also stained sections for tartrate-resistant acid phosphatase to detect osteoclasts. The numbers of osteoclasts remained relatively constant until later times when their numbers decreased (Figure E, F, Phadke et al.). This somewhat surprising loss of osteoclasts was confirmed by histomorphometry (Figure 3A, Phadke et al.).

In summary, (Figure 5, Phadke et al), the trafficking experiments indicated that early after their arrival in the bone, the cancer cells moved to the metaphyseal regions. At least in the mouse, they tended to go to the distal metasphysis before they moved to the proximal. Most cancer cells were cleared from the bone by 24 hr and did not begin to proliferate until after 72 hr. The presence of the cancer cells led to loss of osteoid volume, to a decrease both in the numbers of osteoblasts and osteoclasts. The presence of the cancer cells led to a dramatic restructuring of the bone micro-environment.

This task was completed and the results published.

Task 2. To compare chemotactic properties of metaphyseal bone and marrow with endosteal and cortical bone and marrow .

The second task was to compare the chemotactic properties of metaphyseal bone and marrow with endosteal and cortical bone and marrow. We proposed to prepare bone and marrow cultures; assay breast cancer cells for chemotaxis to the various bone and marrow preparations and assay culture medium from the bone marrow and bone preparations for cytokines and chemokines.

We isolated the femurs from non-cancer bearing mice and divided them into the metasphyses and diaphyses in order to screen for the presence of possible factors that would affect the metastatic cancer cells. The bone pieces and marrow were separated and cultured for 24 hr. The culture media were collected and screened for the presence of cytokines and factors using the RayBio Mouse Cytokine Antibody Array III & 3.1 which can detect 62 different mouse cytokines. Of the 62, we detected at least 15 in the metaphysis and of those 6 were also in the diaphysis (Table 1). Several inflammatory cytokines, IL-6, MIP-2, KC, MCP-1, were present as were adhesion molecules and chemokines. For some, e.g,. IL-6, there appeared to be a gradient between the ends and the mid-section of the bone. We repeated this experiment except that we separated the marrow from the bone and incubated the marrow and the calcified bone separately. We sampled the medium after 12 and 24 hours of culture. More cytokines were present in the 24 hour culture medium than the 12 hour medium. Almost all of the cytokines were strongly present in the culture medium from the calcified metaphyseal bone and not in that from the metaphyseal marrow. These cytokines were not found in the diaphyseal bone or bone marrow. Many of the same inflammatory cytokines were detected in the multiplex assay as in the immunoblot assay.

The Biolplex assay also indicated the presence of G-CSF. An honors student in the laboratory continued to look at G-CSF and also GM-CSF. She found that both were produced primarily by the epiphysis of the bone (Figure 2 Erin Crane2). She went on to show that expression of both molecules was increased in osteoblasts cultured in the presence of conditioned medium from breast cancer cells (Figure 3 Erin Crane4).

Because of the expense we have not yet carried out ELISAs to quantitate all of the detected cytokines. However, we were able to quantitate some of the cytokines with a Bioplex assay (Table 2). A Biorad Bioplex instrument for Luminex Bead assays has just been installed on campus and we plan to quantitate other samples that we have stored frozen.

We plan to carry out a similar experiment with femurs from animals after inoculation of the cancer cells to determine how the cancer cells modify the bone microenvironment. We plan to submit grants to obtain funds to carry out the numerous ELISAs and the chemotactic assays.

Table 1. Cytokines and Growth Factors Detected in the Metaphysis and Diaphysis of Mouse Femurs

Metaphysis	Diaphysis
IL-6	IL-6
L-selectin	L-selectin
P-selectin	P-selectin
Lymphotactin	Lymphotactin
VCAM-1	**VCAM-1**
GCSF	
KC	
MCP-1	
MIP-1α	
MIP-2	
TIMP-1	
IGFPB-5	
sTNFR1 and R2	
INFγ	

Femurs from normal mice were separated into the diaphysis and metasphysis regions and incubated in culture media for 24 hours. The media were assayed with the RayBio Mouse Cytokine Antibody Array III and & 31. Bolded cytokines appeared to be in higher amounts relative to the other cytokines.

Table 2. Cytokine and Chemokine Concentrations from Ex Vivo Cultures of Femurs of Mice.

	Cytokine or Chemokine (pg/ml)						
Femur Component		**KC**	**IL-6**	**MIP-1α**	**IL-1β**	**G-CSF**	**IFN-γ**
	Total Bone, Metaphysis, 12 hours	1276.2	747.4	-	-	252.7	-
	Total Bone, Metaphysis, 24 hours	>8000	5951.5	797.3	81.7	2197	-
	Bone, no marrow, Metaphysis, 12 hours	2658	1009	-	-	229	-
	Bone, no marrow, Metaphysis, 24 hours	>8000	6664.6	626	63.9	2088.5	-
	Bone marrow, Metaphysis, 12 hours	-	-	-	-	-	-
	Bone marrow, Metaphysis, 24 hours	-	-	-	-	-	57.8
	Total bone, Diaphysis, 12 hours	370.4	405.8	-	-	100.7	-
	Total bone, Diaphysis, 24 hours	1915.7	4301.9	-	31.8	550.5	-
	Bone, no marrow, Diaphysis, 12 hours	872	3825.8	-	-	119.5	-
	Bone, no marrow, Diaphysis, 24 hours	1140.5	8099.9	705.4	24	388.3	33.7
	Bone marrow, Diaphysis, 12 hours	117	34.4	-	-	4.3	43.3
	Bone marrow, Diaphysis, 24 hours	262	20.7	-	-	3.5	89.3

Bioplex limits of detection are reported as 1.95–32,000 pg/ml using 4PL or 5PL analysis curves. Media screened as in Table 1 were further analyzed with a Bioplex assay of 18 cytokines. The detected cytokines are shown.

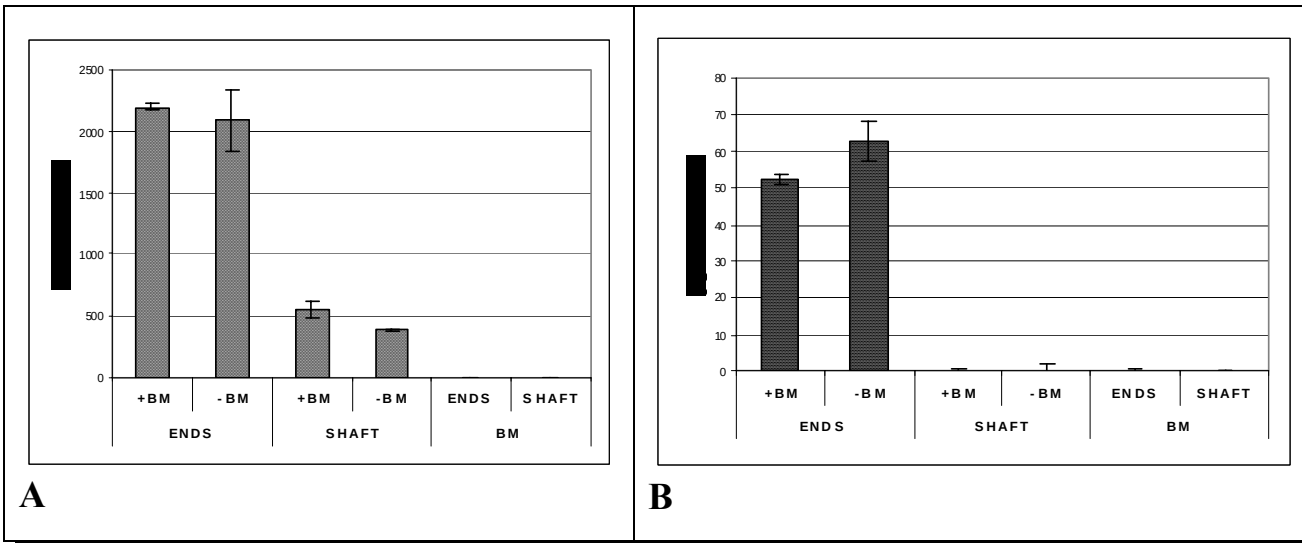

Figure 2: G-CSF, GM-CSF Produced Primarily at Epiphyses

The epiphyses (ENDS) were separated from the diaphyses (SHAFT) (with or without bone marrow), and allowed to incubate for 24 hours. Supernatants were then applied to the BioRad Bioplex ™ Assay. Values are expressed in pg/ml of a.) G-CSF and b) GM-CSF. Error bars represent variation between duplicate samples.

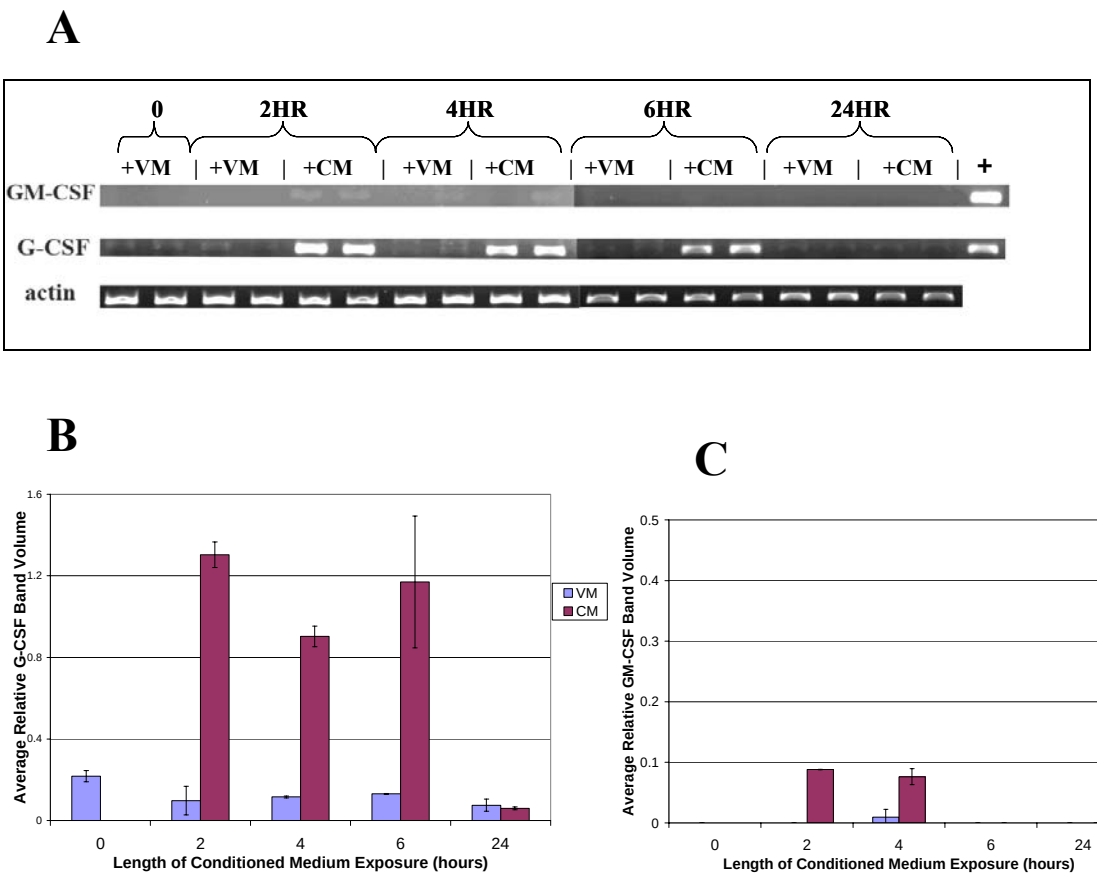

Figure 3 :Conditoned Medium from MDA-MB-231 Cells Rapidly Upregulated G-CSF mRNA in Murine Osteoblasts

(a.) MC3T3-E1 Osteoblasts, plated at $1x10^5$ cells per well in differentiation medium in six well plates for 10 days were treated with 50% MD-MBA-231 CM or 50% VM for 0,2,4,6, or 24 hours in duplicate. After each point, RNA was isolated and a reverse transcriptase (RT) reaction with 0.5 ug RNA was used to create a set of cDNAs. Three separate PCR reactions were subsequently performed on the cDNAs with primers specific for G-CSF, GM-CSF, and actin. All PCR reactions were performed within the optimized linear range of the primer set of interest. PCR products were run on 2% ethidium bromide agarose gels. RNA isolated from MC3T3-E1 cells stimulated with LPS was used as a positive control (+). The intensities of each G-CSF **(b.),** GM-CSF**(c.)** and actin band were measured using ImageJ 1.36b (NIH, USA). Average Relative Band Volume was determined by taking average intensities for duplicate samples divided by respective average actin intensities. Standard deviation represents variation between duplicate samples. This experiment was repeated with similar results.

KEY RESEARCH ACCOMPLISHMENTS

- Determined the pattern of appearance of metastatic breast cancer cells early upon arrival in femurs (1 hr to 6 weeks following inoculation).
- Determined that the cancer cells were found mainly in the metasphyses as opposed to the diaphysis from the earliest times. They also were detected in the distal metaphysis before the proximal metasphysis.
- Determined that tumor cells in the diaphysis were rare except late in the metastatic process. At that time the tumor cells were found in the marrow close to the endosteal bone.
- Quanitated the numbers of metastatic cells in the femur over time using flow cytometry and PCR.
- Determined that osteoblasts in femurs with cancer cell underwent apoptosis and did not differentiate.
- Determined the both osteoblasts and osteoclasts decreased in numbers as the tumor masses increased in size.
- Determined that the metasphyseal bone contains a variety of cytokines and adhesion molecules that were not detected in the diaphyseal bone.

REPORTABLE OUTCOMES

- Michelle Kinder, a Biochemistry and Molecular Biology Major and also an Honors Student in the Schreyer Honors College, worked on part of this project for her honors thesis beginning in her freshman year. She won many awards including a Goldwater Award. She graduated in 2004 and is currently a graduate student at the University of Pennsylvania.

- Elizabeth Chislock, a senior Biochemistry and Molecular Biology Major, also an Honors Student in the Schreyer Honors College, worked on part of this project for her honors thesis. She was the College of Science Student Marshall at graduation entered the graduate program in Molecular Biology of Cancer at Duke University in the fall of 2005.

- A senior Microbiology Major, Shakira Nelson, carried out part of this project for her undergraduate research requirment. She was accepted into a summer undergraduate program at the University of Pittsburgh based on her work. She is employed at the National Library of Medicine and is planning to attend medical school. She is a co-author on the Phadke et al paper.

- Robyn Mercer was a graduate student in Biochemistry and Molecular Biology who worked on various aspects of this project. She graduated in Spring 2005 and is now a postdoctoral fellow at the University of N. Carolina. She is a first author on the published manuscript.

- Karen Bussard as a first year graduate student carried out the Real Time-PCR aspects of this project. She analyzed the data as part of an advanced statistics course. She is a co-author on the manuscript. She is continuing the cytokine analyses described in Task 2.

- Faysal Alqassab, an undergraduate Biology Major, helped to quantitate some of the TRAP staining. He is beginning his senior year.

- Erin Crane, a undergraduate Biochemistry and Molecular Biology major and member of the Schreyer Honors College, worked on the cytokine task. She used the data for her thesis. We plan to incorporate the data into a publication. She will begin medical school at Georgetown fall 2006.

- **Presentations (poster and platform) at the recent Era of Hope meeting.**

Mercer, R.J., P.A. Phadke, J.L. Jewell, C.V. Gay, V. Gilman, D.R. Welch, and **A.M. Mastro**. "Trafficking of breast cancer metastatic cells in bone." Era of Hope, Department of Defense, Breast Cancer Research Program Meeting, June 8-11, 2005, Philadelphia, PA.

Phadke, P.A., R. Mercer, J.F. Harms, J.C. Kappes, Y. Jia, A.R. Frost, **A.M. Mastro**, and D.R. Welch. "Kinetics of the early stages of breast cancer metastasis to bone." Era of Hope, Department of Defense, Breast Cancer Research Program Meeting, June 8-11, 2005, Philadelphia, PA.

Bussard, K.M, P.A. Phadke, R.R. Mercer, J.F. Harms, Y. Jia, J.C. Kappes, A. R. Frost, J.L. Jewell, S. Nelson, C. Moore, C.V. Gay, D.R. Welch, and **A.M. Mastro**. April 1-5, 2006. "Kinetics of metastatic breast cancer cell trafficking in bone." 97th Annual Meeting of the American Association for Cancer Research, Proceedings. 47: 937. Washington, D.C.

- **Publication**

Pushkar A. Phadke*, **Robyn R. Mercer,*** John F. Harms, Yijiang Jia, John C. Kappes, Andra R. Frost, **Jennifer L Jewell**, **Karen M. Bussard**, **Sharkira Nelson**, Cynthia moore, **Carol V. Gay**, **Andrea M. Mastro**# and Danny R. Welch.# Kinetics of Metastatic Breast Cancer Cell Trafficking in Bone. Clinical Cancer Research 12: 1431-1440, 2006 (* equal first authors, # equal senior authors; Mastro, Penn State group is bolded).

CONCLUSIONS

Breast cancer metastatic cells follow a very specific route once in the marrow of the femurs. They either move or are cleared from the diaphysis and migrate to or grow in the metaphysis. In the mouse, they appeared in the distal end before the proximal end of the femur. Later, once

tumor masses formed, the cells were found throughout the marrow cavity. One of the most dramatic findings was the effect of the tumor cells on the osteoblasts. As predicted from our *in vitro* studies, the osteoblasts undergo apoptosis and are unable to function as bone repairing cells. We found in these present studies that *in vivo*, they diminished in numbers in the trabecular bone and that their alkaline phosphatase activity was also greatly reduced compared to bone from control mice. Somewhat unexpected was the finding that the osteoclasts also dimished in number as the tumor masses increased. In addition, we found that the femur contains a variety of cytokines but these are not distributed equally between the two ends. This cytokine distribution may help explain the differences in distribution of cancer cells between the diaphysis and the epiphysis. We plan to determine how these cytokines change in femurs of mice inoculated with the metastatic breast cancer cells. In summary, the metastatic breast cancer cells led to a dramatic restructuring of the bone cells and their microenvironment such that osteolysis was strongly favored. The osteoblasts themselves contribute inflammatory cytokines that affect the environment. The demise in osteoblasts helps to explain why treatment with bisphosphonates to inhibit osteoclasts is insufficient to promote bone healing. Comprehensive treatment needs to include treatment to restore bone matrix as well as to limit osteolysis.

REFERENCES

1. Phadke,* P.A., Mercer* R.R., Harms, J.F., Jia, Y, Frost, Andra R., Jewell, J. L, Bussard, K. M, Nelson, S, Moore, C. M., Kappes, J. C., Gay, C. V., Mastro, A. M., Welch, D. R. Kinetics of Metastatic Breast Cancer Cell Trafficking in Bone. Clinical Cancer Research, 12: 1431- 1440, 2006. * Equal first authors.

2. Body, J.J. Metastatic bone disease: clinical and therapeutic aspects. Bone 13 Suppl 1:S57-S62, 1992.

3. Coleman, R.E. Skeletal complications of malignancy. Cancer. 80: 1588-1594, 1997.

4. Mastro, A.M. Mastro AM, Gay CV, Welch DR, et al. Breast cancer cells induce osteoblast apoptosis: a possiblecontributor to bone degradation. J Cell Biochem 2004;91:265-76.

5. Mercer RR, Miyasaka C, Mastro AM. Metastatic breast cancer cells suppress osteoblast adhesion and differentiation. Clin Exptl Metastasis 2004;21:427-35.

6. Mercer, R.M. and **A.M. Mastro**. 2005. Cytokines secreted by bone-metastatic breast cancer cells alter the expression pattern of f-actin and reduce focal adhesion plaques in osteoblasts through PI 3K. Experimental Cell Research. 310: 270-281.

7. Mundy, G.R. Metastasis to bone: causes, consequences and therapeutic opportunities. Nature Reviews 2: 584-593, 2002.

8. Mason, T.M., B.J. Lord and J.H. Hendry. The development of spatial distributions of CFU-S and *in vitro* CFC in femora of mice of different ages. British Journal of Haematology 73: 455-461, 1989.

9. Harms, J.F., L.R. Budgeon, N.D. Christensen and D.R. Welch. Maintaining GFP Tissue Fluorescence through bone decalcification and long-term storage. Biotechniques 33: 1197-1199, 2002.

10. Muller, A.B. Homey, H. Soto et al. Involvement of chokine receptors in breast cancer metastasis. Nature 140: 50-56, 2001.

Kinetics of Metastatic Breast Cancer Cell Trafficking in Bone

Pushkar A. Phadke,[1] Robyn R. Mercer,[6] John F. Harms,[1] Yujiang Jia,[2] Andra R. Frost,[1,3,5] Jennifer L. Jewell,[6] Karen M. Bussard,[6] Shakira Nelson,[6] Cynthia Moore,[1] John C. Kappes,[2] Carol V. Gay,[6] Andrea M. Mastro,[5,6] and Danny R. Welch[1,3,4,5]

Abstract

Purpose: *In vivo* studies have focused on the latter stages of the bone metastatic process (osteolysis), whereas little is known about earlier events, e.g., arrival, localization, and initial colonization. Defining these initial steps may potentially identify the critical points susceptible to therapeutic intervention.

Experimental Design: MDA-MB-435 human breast cancer cells engineered with green fluorescent protein were injected into the cardiac left ventricle of athymic mice. Femurs were analyzed by fluorescence microscopy, immunohistochemistry, real-time PCR, flow cytometry, and histomorphometry at times ranging from 1 hour to 6 weeks.

Results: Single cells were found in distal metaphyses at 1 hour postinjection and remained as single cells up to 72 hours. Diaphyseal arrest occurred rarely and few cells remained there after 24 hours. At 1 week, numerous foci (2-10 cells) were observed, mostly adjacent to osteoblast-like cells. By 2 weeks, fewer but larger foci ($\geq$50 cells) were seen. Most bones had a single large mass at 4 weeks (originating from a colony or coalescing foci) which extended into the diaphysis by 4 to 6 weeks. Little change ($<$20%) in osteoblast or osteoclast numbers was observed at 2 weeks, but at 4 to 6 weeks, osteoblasts were dramatically reduced (8% of control), whereas osteoclasts were reduced modestly (to $\sim$60% of control).

Conclusions: Early arrest in metaphysis and minimal retention in diaphysis highlight the importance of the local milieu in determining metastatic potential. These results extend the Seed and Soil hypothesis by demonstrating both intertissue and intratissue differences governing metastatic location. Ours is the first *in vivo* evidence that tumor cells influence not only osteoclasts, as widely believed, but also eliminate functional osteoblasts, thereby restructuring the bone microenvironment to favor osteolysis. The data may also explain why patients receiving bisphosphonates fail to heal bone despite inhibiting resorption, implying that concurrent strategies that restore osteoblast function are needed to effectively treat osteolytic bone metastases.

Authors' Affiliations: Departments of [1]Pathology and [2]Medicine-Hematology/Oncology, [3]Comprehensive Cancer Center, [4]Center for Metabolic Bone Disease, [5]National Foundation for Cancer Research, Center for Metastasis Research, University of Alabama at Birmingham, Birmingham, Alabama, and [6]Department of Biochemistry and Molecular Biology, Pennsylvania State University, University Park, Pennsylvania

Received 8/19/05; revised 11/1/05; accepted 12/15/05.

Grant support: U.S. Army Medical Research and Materiel Command (DAMD-17-02-1-0541, DAMD-17-03-01-0584, and DAMD 17-02-1-0358) and the University of Alabama at Birmingham Breast Specialized Programs of Research Excellence (P50-CA89019). Additional support was provided by CA87728, the National Foundation for Cancer Research, Center for Metastasis Research, and the Pennsylvania Department of Health Breast Cancer Program.

The costs of publication of this article were defrayed in part by the payment of page charges. This article must therefore be hereby marked *advertisement* in accordance with 18 U.S.C. Section 1734 solely to indicate this fact.

Note: P.A. Phadke and R.R. Mercer contributed equally to this work.

This work was submitted in partial fulfillment of the requirements for the University of Alabama at Birmingham Graduate Program in Molecular and Cellular Pathology (P.A. Phadke) and Penn State Graduate Program in Biochemistry and Molecular Biology (R.R. Mercer).

Requests for reprints: Danny R. Welch, Department of Pathology, University of Alabama at Birmingham, Volker Hall G-019A, 1670 University Boulevard, Birmingham, AL 35294-0019. Phone: 205-934-2961; Fax: 205-975-1126; E-mail: DanWelch@uab.edu.

doi:10.1158/1078-0432.CCR-05-1806

Breast cancer has a remarkable predilection to colonize bone, with an incidence between 70% and 85% in patients (1–3). At the time of death, metastatic bone disease accounts for the bulk of tumor burden (4). For women with bone metastases, the complications—severe, often intractable pain, pathologic fractures, and hypercalcemia—are catastrophic. Despite its obvious clinical importance, very little is understood about the fundamental mechanisms responsible for breast cancer metastasis to bone. Research progress has been hampered by the dearth of, and technical difficulties inherent in, the current models.

Most models of metastasis poorly recapitulate the pathogenesis of breast cancer. The ideal model would involve dissemination from an orthotopic site (i.e., mammary fat pad), colonization, and osteolysis. None of the currently available human breast xenograft models spread to bone following orthotopic implantation and only one murine model metastasizes to bone from the mammary fat pad (5). Furthermore, most human cell lines do not metastasize to bone in mice regardless of route of injection. The most commonly used model of breast cancer metastasis to bone involves injection of tumor cells into the arterial circulation via the left ventricle of the heart (4, 6–8). This route of injection minimizes first-pass filtration through pulmonary capillaries, thereby allowing more cells to reach the bone.

Current methods to detect bone metastases are insufficiently sensitive (e.g., radiography) or are impractical for adequately statistically powered experiments because of costs or labor-intensiveness. Radiography can detect osteolytic lesions only after more than half of the calcified bone matrix has been degraded (9). Microcomputerized tomography is not widely available, but is likewise of insufficient resolution to recognize single tumor cells. Serial sectioning (which would be required to locate rare single cells) is cost-prohibitive, except for small studies. As a result, experiments have been limited to late events of metastatic bone disease, such as osteolysis. Therefore, antecedent events (i.e., arrival, lodging, intraosseous trafficking, and colonization) have not been studied except by inference.

To overcome some of the technical limitations, more sensitive methods using reporter molecules, such as luciferase (10) or β-galactosidase (LacZ) have recently been described (11–13). Luciferase, although it allows for *in situ* detection of tumor cells in the bone, does not allow for microscopic localization of the cells. Because luminescence depends on a fully viable cell, use of luciferase is limited *ex vivo*. β-Galactosidase is excellent for studies at the histologic level but cannot be used for studies involving intact bone unless the lesions are macroscopic. Diffusion or distribution of substrate into bone is also a complication.

Fluorescent molecules, like enhanced green fluorescent protein (GFP), have also been employed with some success in the early detection of bone metastasis (14–16). We recently used the GFP-tagged MDA-MB-435 metastatic human breast cancer cell line to reveal formation of osteolytic bone lesions following intracardiac injection in athymic mice (15). Like luciferase, GFP can be used to detect lesions *in situ*, even though the limits of detection are restrictive (~0.5-1 mm). During experiments designed for other purposes, we detected single tumor cells in bone within minutes postinjection. Because to the best of our knowledge, no one had ever systematically studied the earliest tumor cell-bone interactions (except by serendipitous histologic sections), we decided to use the power of GFP to begin addressing the early events associated with breast tumor cells that have already disseminated to bone.

It has long been recognized that, once cells arrive in the bone, they alter homeostasis. Turnover of the skeleton is dynamic and continuous throughout embryonic development and adulthood. Calcified bone matrix turns over completely, on average, every decade (17, 18). Calcified matrix remodeling involves an interplay between osteoblasts (bone forming cells) and osteoclasts (bone resorbing cells). Altering the balance of activities results either in excessive bone deposition (osteopetrosis) or bone loss (osteoporosis). Although larger individual bone lesions contain regions that are both osteopetrotic and osteoporotic, most breast cancer bone metastases are not osteolytic. The current paradigm suggests that tumor cells influence osteoclast activity (4, 19). Using the GFP model of breast cancer metastasis to bone, we sought to identify key tumor cell–bone cell interactions (and the timing of those interactions) that occur during the pathogenesis of bone metastasis.

Materials and Methods

Cell lines and culture. Metastatic human breast carcinoma cell line, MDA-MB-435 (MDA-435), a generous gift from Dr. Janet Price (University of Texas M.D. Anderson Cancer Center, Houston, TX), was stably transfected with pEGFP-N1 (BD Biosciences Clontech, Palo Alto, CA) by electroporation (Bio-Rad Model GenePulser, Hercules, CA; 220 V, 960 μ Fd, $\infty\Omega$) or transduced with a HIV type 1-based, lentiviral vector system constitutively expressing enhanced GFP (20, 21). For the lentivirus, the GFP coding sequence was inserted into the vector 5′ of the internal ribosome entry site and puromycin sequences, each of which were under control of the early cytomegalovirus promoter. Infectious stock were prepared by transfection of 293T cells and used at a multiplicity of infection of ~10.

The origin of MDA-MB-435 has been questioned because the cells express melanoma-associated genes in cDNA microarray experiments. However, the patient was reported only to have a breast carcinoma. Because MDA-MB-435 cells express milk proteins (22), it is most simple to conclude that the cells are poorly differentiated breast carcinoma.

Parental cells were cultured in a mixture (1:1 vol/vol) of DMEM and Ham's F12 media (DMEM/F12; Invitrogen, Carlsbad, CA) supplemented with 2 mmol/L L-glutamine, 1 mmol/L sodium pyruvate, 0.02 mmol/L nonessential amino acids, 5% fetal bovine serum (Atlanta Biologicals, Norcross, GA), without antibiotics or antimycotics (cDME/F12). All cultures were confirmed to be negative for *Mycoplasma* spp. infection using a PCR-based test (TaKaRa, Shiga, Japan).

GFP-expressing cells were grown in cDME/F12 plus G418 (Geneticin, 500 μg/mL, Invitrogen) or puromycin (500 μg/mL, Fisher Scientific, Hampton, NH). The brightest 15% (lentiviral) or 25% (pEGFP) fluorescing cells were sorted using either Coulter EPICS V cell sorter (Beckman-Coulter, Fullerton, CA) or a BD FACSaria cell sorter (BD Biosciences Immunocytometry Systems, San Jose, CA).

Intracardiac injections. Cells at 80% to 90% confluency were detached using a mixture of 0.5 mmol/L EDTA and 0.05% trypsin in Ca^{+2}-, Mg^{+2}-, and $NaHCO_3$-free HBSS. Viable cells were counted using a hemacytometer and resuspended at a final concentration of 1.5×10^6 cells/mL in ice-cold HBSS. Cells were not used unless viability was >95%, but was usually >98%. Female athymic mice ages between 4 and 6 weeks (Harlan Sprague-Dawley, Indianapolis, IN) were anesthetized by i.m. administration of a mixture of ketamine-HCl (129 mg/kg), and xylazine (4 mg/kg). Cells (3×10^5 in 0.2 mL) were injected into the left ventricle of the heart between the third and fourth or between the fourth and fifth intracostal space. The presence of bright red, as opposed to burgundy, colored blood prior to and at the end of each inoculation confirmed injection of the entire volume into the arterial system. Mice were necropsied at 1, 2, 4, 8, 24, 48, and 72 hours and 1, 2, 4, and 6 weeks postinoculation following anesthesia with ketamine/xylazine and euthanasia by cervical dislocation. At least two independent experiments were done with 5 to 12 mice per experimental group. Not all time points were collected for every experiment.

Although widespread skeletal metastases develop after intracardiac injection (15, 23), the experiments reported here focused exclusively on the femur, a common site for metastasis that is easily accessible. The femurs were removed and examined by low magnification (×2-10) fluorescence stereomicroscopy and histologic and histomorphometric analyses (24, 25). Some femurs were divided into proximal and distal metaphyses plus cortical shaft (diaphysis) from which the marrow was collected and cells examined by flow cytometry or quantitative real-time PCR. Corroborating experiments were done with the contralateral femur to assure that there was no bias for sidedness.

Mice were maintained under the guidelines of the NIH, the University of Alabama at Birmingham, and the Pennsylvania State University. All protocols were approved and monitored by the appropriate Institutional Animal Care and Use Committees.

Fluorescence microscopy. To visualize metastases derived from the GFP-tagged cell lines, whole femurs (dissected free of soft tissue using a no. 11 scalpel blade with gauze used to grip and remove tissue remnants) were placed into Petri dishes containing ice-cold Ca^{+2}- and Mg^{+2}-free Dulbecco's PBS and examined by fluorescence microscopy using a Leica MZFLIII dissecting microscope with ×0.5 objective and

GFP fluorescence filters ($\lambda_{excitation}$ = 480 ± 20 nm; $\lambda_{emission}$, 510 nm barrier; Leica, Deerfield, IL). Photomicrographs were collected using a MagnaFire digital camera (Optronics, Goleta, CA), and ImagePro Plus 5.1 software (Media Cybernetics, Silver Spring, MD).

Bone fixation and storage. Intact, dissected femurs from individual mice were placed in 25 mL glass scintillation vials and fixed in freshly prepared 4% paraformaldehyde in Ca^{+2}- and Mg^{+2}-free Dulbecco's PBS or in periodate-lysine-paraformaldehyde solution (26) at 4°C for 24 to 48 hours. GFP fluorescence was difficult to maintain in fixed tissues and bone sections; however, we were able to overcome this limitation by maintaining the samples at 4°C (27). Bones destined for histologic sectioning were subsequently removed and decalcified in 0.5 mol/L EDTA in Ca^{+2}- and Mg^{+2}-free Dulbecco's PBS.

Bone histomorphometry. Bones were dehydrated in increasing concentrations of ethanol and embedded in a mixture of 80:20 methyl methacrylate and dibutylphthalate. Serial coronal sections (5 μm) were obtained using a Leica 2265 microtome. The distal ends of femurs (spongiosa) were analyzed. Sections were first stained with Sanderson's rapid bone stain for 2 minutes. Once tumor cells were identified, subsequent sections were stained with Goldner's trichrome and tartrate-resistant acid phosphatase (TRAP). Histomorphometry was done at the University of Alabama at Birmingham Center for Metabolic Bone Disease Histomorphometry and Molecular Analysis Core Facility by the method of Parfitt et al. (24, 25) using Bioquant image analysis software (R&M Biometrics, Nashville, TN).

Immunohistochemistry. Paraffin-embedded samples were sectioned (5 μm, coronal or sagittal), deparaffinized, and rehydrated before antigen retrieval by microwaving for ~8 minutes at full power (700 W) in a 10 mmol/L citrate buffer (pH 6). Samples were boiled for 5 minutes in the microwave oven. Endogenous peroxidase activity was blocked by treatment with 3% hydrogen peroxide for 5 minutes. Sections were blocked with 1% goat serum for 1 hour. Slides were incubated with primary rabbit polyclonal anti-GFP IgG (1:250; Molecular Probes, Eugene, OR) for 1 hour, followed by secondary biotinylated anti-rabbit antibody (TITRE; Level 2 Ultra Streptavidin Detection System, Signet Labs, Dedham, MA). Detection was achieved using Biogenex liquid DAB kit (Biogenex, San Ramon, CA) and slides were counterstained using hematoxylin. GFP-positive tumor samples served as positive controls. Negative controls were done by omitting the primary antibody.

Some femurs were fixed in a solution of 2% paraformaldehyde containing 0.075 mol/L lysine and 0.01 mol/L sodium periodate (pH 7.4), 4°C for 24 hours in an attempt to maintain alkaline phosphatase activity (26). Although the alkaline phosphatase activity was not well preserved, fluorescence was maintained; fluorescent MDA-435^{GFP} cells could be observed in femurs taken throughout the time course. Following decalcification as described above, the bones were embedded in paraffin. Paraffin-embedded bones were sectioned lengthwise into 10 μm sections and several sections throughout the bone were analyzed. The sections were deparaffinized, rehydrated, and stained for apoptotic cells with a modified terminal nucleotidyl transferase–mediated nick end labeling (TUNEL) procedure using Cy-5 rather than FITC-labeled dUTP (28). Bone sections were first scanned at ×20 magnification using a fluorescence confocal microscope. Areas in which GFP-positive cells were detected were further analyzed at ×40 magnification with both fluorescence and phase microscopy. Fluorescent images were captured at two wavelengths $\lambda_{excitation}$ = 480 ± 20 nm ($\lambda_{emission}$, 520 nm for GFP) and $\lambda_{excitation}$ = 647 nm ($\lambda_{emission}$, 670 nm for Cy-5). A comparison of the numbers of breast cancer cells detected by fluorescence microscopy versus use of anti-GFP gave essentially the same trends (data not shown).

TRAP-positive cells were determined in the femurs of mice at various times following inoculation with metastatic breast cancer cells. Two to eight sections from two to four bones per time period were stained for the presence of TRAP by immunohistochemistry (Sigma-Aldrich, St. Louis, MO). After staining, the sections were viewed with a fluorescent light microscope at ×20 magnification. Three images (1,349 pixels/500 μm) from the distal end and three images from the proximal end were collected and converted into JPEG format. The number of TRAP-positive cells was counted in each image. The Image J program (NIH) was used to calculate the bone area in each field.

Some decalcified femurs were cryosectioned and stained for alkaline phosphatase activity (Sigma-Aldrich). The sections were examined with a light microscope, the images digitally collected, and analyzed for the amount of alkaline phosphatase stain per area of bone at the growth plate and in the trabecular region. The data were calculated as ratio of the mm^2 of the alkaline phosphatase stain to mm^2 of bone.

Flow cytometric and DNA analysis. Femurs were removed from five to six mice at each time and cut into the distal and proximal metaphyses and the diaphysis. Bone marrow was flushed from these regions with a 1 mL tuberculin syringe fitted with a 26-gauge needle. The marrow in the center of the diaphysis was collected separately from the endosteal marrow close to the cortical bone as previously described (29). For flow cytometry, the RBC were lysed with ACK solution (15 mmol/L NH_4Cl, 1 mmol/L $KHCO_3$, 0.1 mmol/L Na_2 EDTA) and the remaining cells were fixed with 2% paraformaldehyde. Samples were stored at 4°C until they were analyzed by flow cytometry (Coulter XL-MCL) using standardized fluorescent beads (10 μm; Sphero AccuCount Rainbow Fluorescent particles, Spherotech, Libertyville, IL) to estimate the total number of cancer cells present. Standard curves were also generated by adding known numbers of MDA-MB-435 cells to mouse bone marrow cells. The samples of the mixtures of cells were prepared in the same way as the experimental samples. A background value of 200 cells was determined from the data obtained from the control animals in which no GFP-positive cells were present.

For DNA analysis, marrow was centrifuged and frozen in Ca^{+2}- and Mg^{+2}-free Dulbecco's PBS. At a later time, DNA was prepared from the samples with a DNeasy kit (Qiagen, Valencia, CA). The DNA was subjected to quantitative real-time PCR (Nucleic Acid Facility, Penn State, University Park, PA) using primers to detect the *HERVK* gene (human endogenous retrovirus, group K), a gene found in the human but not in the mouse genome (30). To establish a standard curve, MDA-435^{GFP} cells were counted, diluted, and added to preparations of mouse bone marrow cells. DNA was isolated from these samples and treated as the experimental samples for PCR. Although one cell could be detected in the standard curve samples, a more conservative cutoff of 150 cells was used due to practical considerations, i.e., cell extract volumes and variations in the amount of mouse DNA present in each sample.

Statistics. Each series of injections involved between 5 and 15 mice per experimental group or time. Femurs were apportioned for various subsequent analyses. Comparisons between groups were done by one-way ANOVA with Student-Neumann-Kuels or Tukey's post-tests. Statistical significance was defined as a probability $P \leq 0.05$.

Results

Kinetics of MDA-435^{GFP} tumor cells trafficking in the bone. Numerous solitary fluorescent cells could be visualized in the intact bone (i.e., the bone is not cut, but has been stripped of surrounding muscle) 1 hour following intracardiac injection using fluorescence microscopy (Fig. 1A1). The majority (>90%) of cells were found in the metaphyseal regions, not in the diaphysis, by fluorescence. Routine identification of single tumor cells using H&E stain, although possible, proved difficult. Even with evidence that tumor cells were present in the bone (i.e., by fluorescence), we could not always unambiguously identify single tumor cells in histologic sections stained by H&E.

To facilitate detection of solitary tumor cells by histology and to determine their positions within the trabeculae, cellular

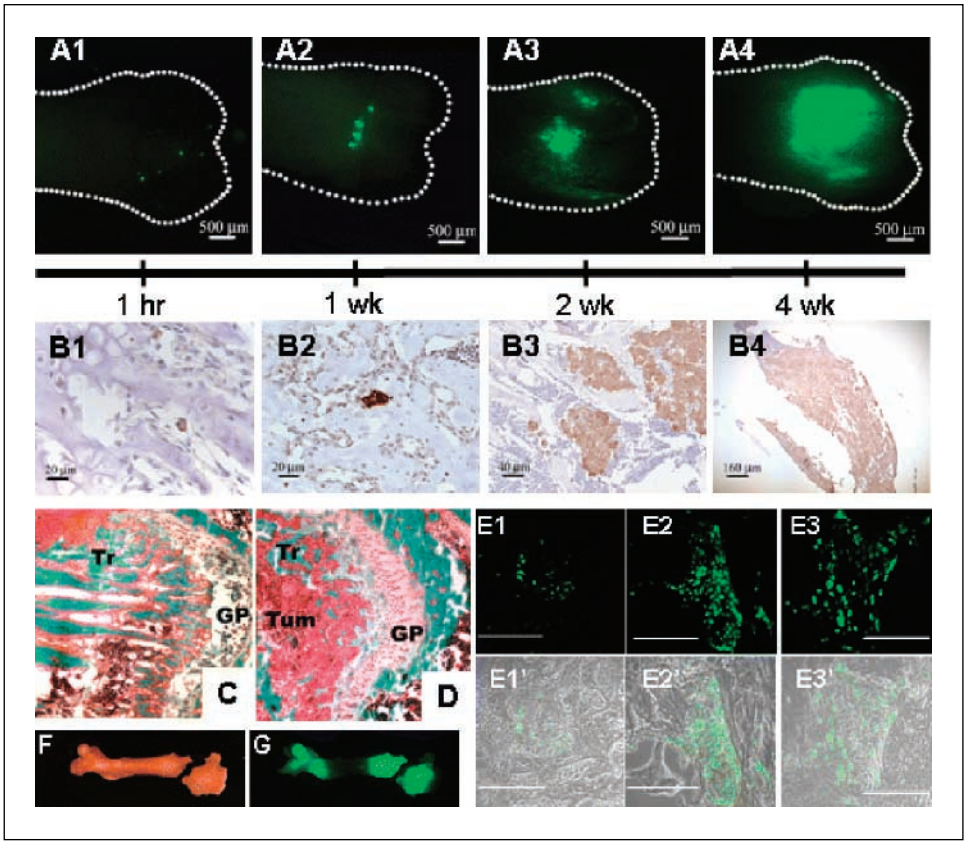

Fig. 1. The kinetics of MDA-435^{GFP} metastatic growth in the femur following intracardiac injection. Whole femurs were dissected and fluorescent foci were visualized in the intact bones using a fluorescent stereomicroscope. *A,* fluorescent foci were observed, mainly in the distal end of femurs, as shown at 1 hour (*A1*), 1 week (*A2*), 2 weeks (*A3*), and 4 weeks (*A4*). *B,* MDA-435^{GFP} cells were detected by anti-GFP immunohistochemistry (*brown staining cells*) in femurs at 1 hour (*B1*, single cell), 1 week (*B2*, clusters of two to three cells), 2 weeks (*B3*), and 4 weeks (*B4*). With time, the number of fluorescent foci decreased as the size increased. Independent tumor deposits often coalesced. *C* and *D,* representative images of distal ends of femur stained with Goldner's trichrome stain (*C,* normal bone; *D,* 4 weeks). The amount of trabecular bone (*Tr*, stained teal) is significantly lower in bone containing tumor cells, reflective of osteolytic degradation. Tumor cells (*Tum*) infiltrating the metaphyseal area near epiphyseal growth plate (*GP*) are labeled for reference. *E,* fluorescent tumor cell foci in trabecular bone in paraffin-embedded sections at 2 weeks (*E1*), 4 weeks (*E2*), and 6 weeks (*E3*) postinjection. Magnification line indicates 100 μm. E1′, E2′, and E3′ are composites of fluorescent and phase images. Representative bright field (*F*) and fluorescent (*G*) images of a mouse femur at 4 weeks show two large metastatic foci, one at each end. The distal end shows an iatrogenic fracture, presumably due to weakness caused by tumor cell – induced osteolysis.

location was estimated in two dimensions using fluorescence. Then, serial histologic sections were cut from the regions exhibiting fluorescence. Although this manipulation increased the odds of finding sections containing single cells, it was not always possible to detect cells in every 5 to 10 μm section stained using anti-GFP antisera. Nonetheless, as implied by the fluorescence data, most tumor cells were located in the primary spongiosa of the metaphysis of the distal femur (Fig. 1B and E). Although fluorescent cells were not frequently detected in the femoral head at 1 hour postinjection, some GFP-positive cells were detected by immunohistochemistry (data not shown). There was no evidence of unusual inflammation or immune cell infiltration at the sites of tumor cell arrest or colonization.

In a third, parallel approach, we detected cells without visualization constraints or sampling errors associated with sectioning, instead quantifying tumor cells in various marrow compartments using flow cytometry or real-time PCR. Separation of the marrow from metaphyses and diaphysis followed by flow cytometry or real-time PCR to detect MDA-435^{GFP} cells revealed a slightly different pattern of tumor cell distribution within the bone at the early times, but an entirely consistent pattern of distribution at the later times (Fig. 2). These methods were limited because precise separation of the diaphysis from the metaphysis was not consistent. Therefore, cancer cells at the interface between bone regions could not be localized with certainty. Histologic sections confirmed precise localization (Fig. 1). As a whole, the various methods to assess localization were largely confirmatory. In addition, we also determined that cancer cells in the diaphysis were mostly located next to the endosteal bone rather than in the marrow in the center of the shaft. By 4 to 6 weeks, >95% of tumor cells were found in the endosteal marrow (Fig. 5).

Of the 3×10^5 cells injected per mouse, a small fraction were detectable in the femurs (Table 1), as expected, because cells are distributed throughout the body following injection into the arterial circulation. Flow cytometry and real-time PCR were used to quantify the number of cells present. Cells were flushed from the marrow space in the metaphyseal and diaphyseal regions and examined by flow cytometry to detect GFP-tagged cells (Fig. 2). In addition, DNA isolated from the bone marrow was analyzed for the presence of human DNA by real-time PCR using a human-specific primer/probe set (Fig. 2). Regardless of the method, seeding of the femurs with breast cancer cells was rare (44 ± 6 cells; 0.01% per femur; Table 1). As a result, the absolute numbers were highly variable between mice and between techniques. Thus, the total number of single cells identified was not sufficient to perform statistical analyses with adequate power. Nonetheless, we did observe several consistent changes. First, solitary cells in the diaphysis were seldom detected beyond 24 hours in any of the mice, until metaphyseal lesions had apparently extended into the diaphyses at later times (Figs. 1G and 2). Second, the number of fluorescent foci (i.e., cell masses) detected by fluorescent stereomicroscopy decreased progressively beginning from 1 to 72 hours. This result is consistent with the clearance of disseminated tumor cells from other organs (31, 32). Third, single cells persisted in the femur for up to 72 hours. In general, evidence of cell division prior to 72 hours postinoculation was infrequent.

Whereas initial proliferation of arrested cells was delayed, distinct metastatic foci (5 ± 1) were easily detected by fluorescence microscopy of the intact bone (Fig. 1A2) as well as immunohistochemistry in the femur at 1 week (Fig. 1B2) and fluorescence microscopy of bone sections (Fig. 1E). Most of the foci were small and consisted of <10 cells (i.e., only three to four cell divisions). Although most metastatic lesions were localized at the distal end, a fraction of the bones had fluorescent foci growing at the proximal ends as well.

By 2 weeks, larger but fewer foci (2.8 ± 0.5) were detected at the distal end (Fig. 1A3 and B3). The foci were comprised of clusters of ~50 cells. These progressively increased in size and decreased in number to an average of one metastatic focus at 4 weeks, presumably by coalescence (Fig. 1A4, B4, and G). By 6 weeks, tumor cells directly extended into the diaphysis, and in some cases, the whole medullary canal was occupied by tumor. Histomorphometry of the lesions revealed loss of most trabecular bone by 4 to 6 weeks (compare Fig. 1D and Fig. 1C).

Tumor cell modification of the bone microenvironment. Histomorphometric analysis further showed specific modification of the microenvironment when tumor cells were present (Fig. 3). We had previously shown that MDA-435^{GFP} cells form radiographically detectable osteolytic lesions within 4 to 6 weeks following intracardiac injection (15). That finding was corroborated by histomorphometry showing that calcified bone volume decreased as tumor volume increased

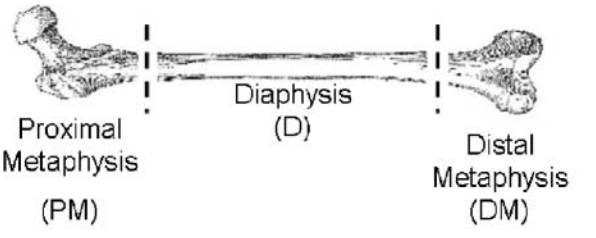

Time after injection	Flow cytometry			Real-time PCR		
	PM	D	DM	PM	D	DM
1 hr	1/5	2/5	0/5	4/5	3/5	2/5
4hr	2/5	2/5	0/5	4/5	4/5	3/5
24 hr	0/5	0/5	0/5	0/4	4/4	0/4
72 hr	2/5	1/5	2/5	2/5	4/5	1/5
1 wk	1/5	1/5	0/5	3/5	5/5	4/5
4 wk	2/5	2/5	3/5	4/5	5/5	5/5
6wk	0/3	1/3	2/3	2/3	3/3	3/3

Femoral ends were separated from the shaft with scissors. The proximal (PM) and distal (DM) metaphyses and the diaphysis (D) were flushed with ice-cold saline. Cells were collected and prepared for flow cytometry or DNA isolation and subsequent analysis by real-time PCR using HERVK, a human-specific gene. In practice, the limit of detection of MDA-435^{GFP} cells by flow cytometry was ~200 cells; by PCR it was ~150 cells. Shown are the numbers of animals in which the cancer cells were detected at various times and the bone areas in which they were found. The denominator is the number of bones examined at each time. Please note: the data presented are incidence only. The calculated number of cells is presented in Table 1 for each time.

Fig. 2. Detection of MDA-435^{GFP} metastatic cells by flow cytometry or real-time quantitative PCR in the metaphyseal and diaphyseal ends of the femur at various times following intracardiac inoculation.

Table 1. Retention of MDA-435^{GFP} cells in the femur following intracardiac injection

Time postinjection	Number of MDA-435^{GFP} cells in the femur
	Geometric mean (±1 SD)
1 h	41 (16-104)
4 h	54 (5-529)
24 h	40 (7-270)
72 h	44 (11-180)
1 wk	41 (20-82)
4 wk	11,271 (2,893-43,915)

NOTE: Marrow containing tumor cells was isolated from femurs as described in Materials and Methods. The number of MDA-435^{GFP} cells was determined by real-time quantitative PCR using probes for the human gene, HERVK. Shown are log-transformed data for four to five mice per group and only mice containing MDA-MB-435^{GFP} cells were included in the analysis.

(Fig. 3A). A decrease of 97% in the ratio of osteoid surface to bone surface at the 4-week point to osteoblast loss or loss-of-function as a major contributor to the decrease in calcified bone volume. This finding is consistent with previous work showing that MDA-MB-435 and MDA-MB-231 cells induce osteoblast apoptosis (33) and retard osteoblast differentiation (34) *in vitro*.

Importantly, osteoblast number per trabecular bone surface area in the metastatic lesions decreased with time (Fig. 3B). Bones from uninjected, age-matched mice served as negative controls. By 2 weeks, the number of osteoblasts decreased by ~20% in tumor-bearing mice. By 4 weeks, however, the decrease was more dramatic (~92% decrease; Fig. 3B). The decrease in osteoblast number was accompanied by an increase in the number of apoptotic osteoblasts observed by TUNEL (Figs. 3D and G, and 4A). Apoptotic osteoblasts were found at both proximal and distal ends of the femur, but little change in the number of apoptotic osteoblasts was observed in the diaphysis until tumor cells were routinely observed in that portion of the bone (Fig. 4A). This finding suggested that osteoblast apoptosis was occurring mostly when tumor cells were present. Supporting this hypothesis, TUNEL-positive osteoblasts were found almost exclusively in the presence (≤50 μm) of GFP-positive breast cancer cells (Figs. 3G and 4B). Previous (33) and current experiments (data not shown) have shown almost no tumor cell apoptosis when adjacent to osteoblasts. Bone sections stained for alkaline phosphatase, a marker for osteoblasts, showed a dramatic decrease as tumor burden increased (Fig. 3H-J). The ratio of the area occupied by alkaline phosphatase-positive cells per area of trabecular bone in the femurs of cancer-bearing mice was significantly lower compared with healthy mice (2.0 ± 0.6 versus 9.6 ± 1.7, respectively; $P \leq 0.0001$). In contrast, alkaline phosphatase activity in chondrocytes located in the growth plate was not significantly different (control, 25.9 ± 4.7; tumor bearing, 24.1 ± 5.0).

The number of osteoclasts remained unchanged at 2 weeks, but unexpectedly, a consistent decrease (~35-40% or to 60%

of control) in osteoclast number was observed at later times (Fig. 3C). This difference was evident by both quantitative histomorphometric analysis (Fig. 3C) and TRAP staining (Fig. 3E and F). The absolute number of both cell populations decreased so that the ratio of osteoblasts to osteoclasts decreased from an average of 40 to only 4 by 4 weeks.

Discussion

Bone is the most common site for metastases from breast carcinomas and their sequela account for approximately two-thirds of the costs associated with treating women with the disease (4, 36). As with most metastases, symptoms occur relatively late in disease progression. Whereas prevention of metastases altogether is ideal, restriction of progression to an asymptomatic state would improve clinical management of breast cancer. Likewise, repair of already existing lesions would benefit patients whose disease progression has been halted. As a result, understanding the antecedent steps for bone metastasis and osteolysis should provide insights for developing therapeutic interventions.

The results presented here are, to the best of our knowledge, the first to describe the behavior of breast cancer cells at the earliest times after they have arrived in the femur. Although the femur may not represent the behavior of tumor cells in all bones, it is a common site of secondary colonization both in patients with breast cancer and in experimental models. Therefore, we considered it an appropriate site for studying the process.

Single tumor cells were detected in the femur 1 hour after introduction into the arterial circulation (Fig. 5B). It is noteworthy that, even at this early time, tumor cells arrested primarily in the metaphyses rather than diaphyses. Although it is possible that differential expression of adhesion molecules may be found in metaphyseal versus diaphyseal bone

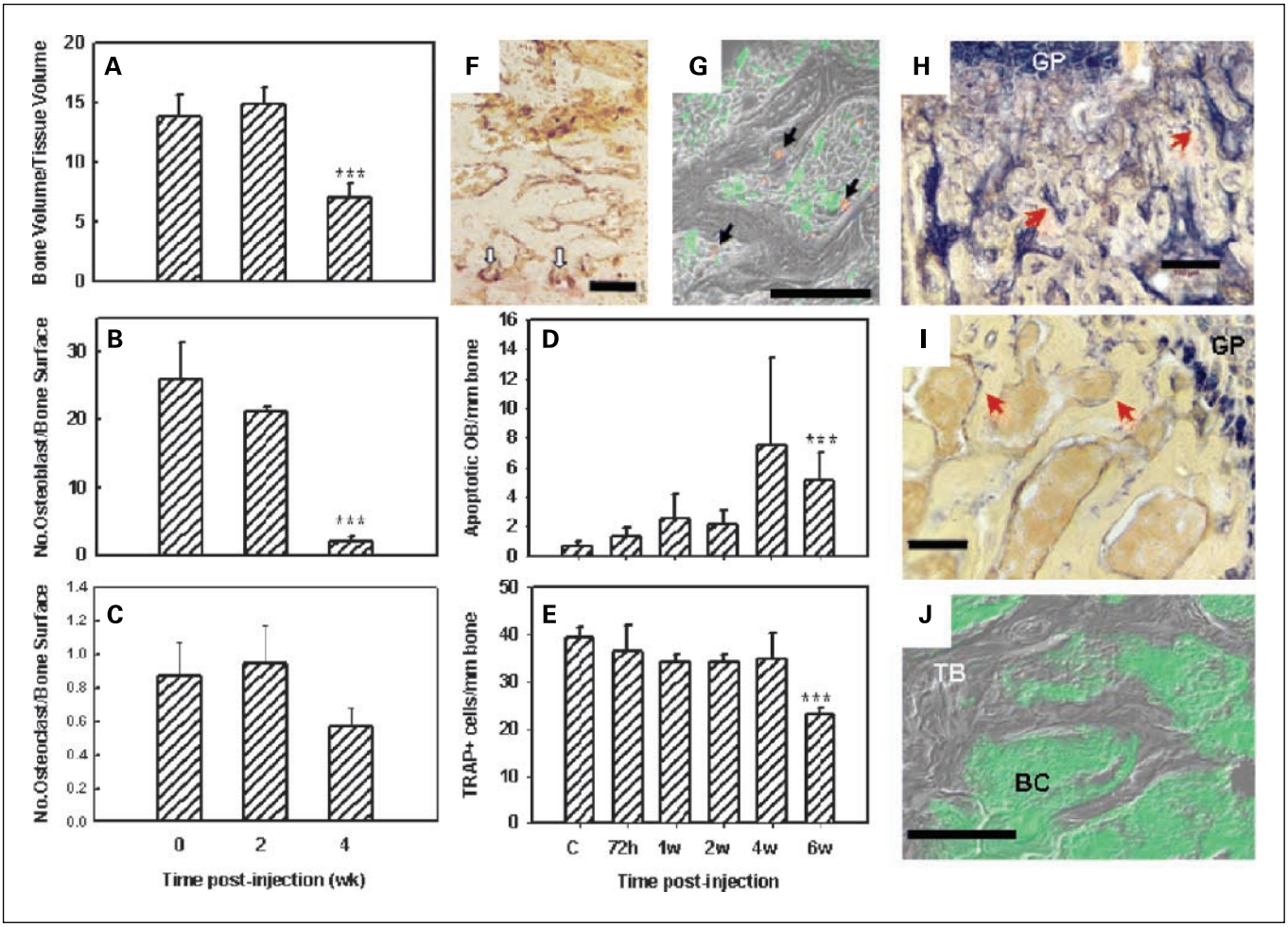

Fig. 3. MDA-435^{GFP} breast cancer cells diminished osteoblast and osteoclast numbers in colonized bone as evaluated by quantitative bone histomorphometry, immunohistochemistry, and fluorescent microscopy. *A-C,* histomorphometric analyses (*A,* bone volume to tissue volume; *B,* number of osteoblast per bone surface; *C,* number of osteoclast per bone surface). *D,* the number of apoptotic osteoblast (TUNEL-positive) per linear bone surface at times following inoculation of tumor cells. *E,* the number of osteoclasts (staining for TRAP) per linear bone surface at times following inoculation of tumor cells. *A-E,* significantly different ($P \leq 0.05$) from normal bone. *F,* representative image of osteoclast staining for TRAP (*red stain with white arrows*) taken from a section of femur 2 weeks after tumor cell inoculation. *G,* merged photomicrograph of MDA-435^{GFP} tumor cells (*green*) surrounding apoptotic osteoblast (*red*, TUNEL using Cy-5 probe) taken from a femur 6 weeks following inoculation. *H, I, J,* cryosections from a femur taken 4 weeks after tumor inoculation. *H,I,* stained for alkaline phosphatase activity (*blue staining by red arrows*) indicative of osteoblast; *J,* merged fluorescent and phase images showing trabecular bone (*TB*) surrounded by MDA-435^{GFP} cells (*BC*). Alkaline phosphatase activity was greatly diminished in the trabecular bone of tumor-bearing femurs but was still present in the growth plate (*GP*). Bars, 100 μm.

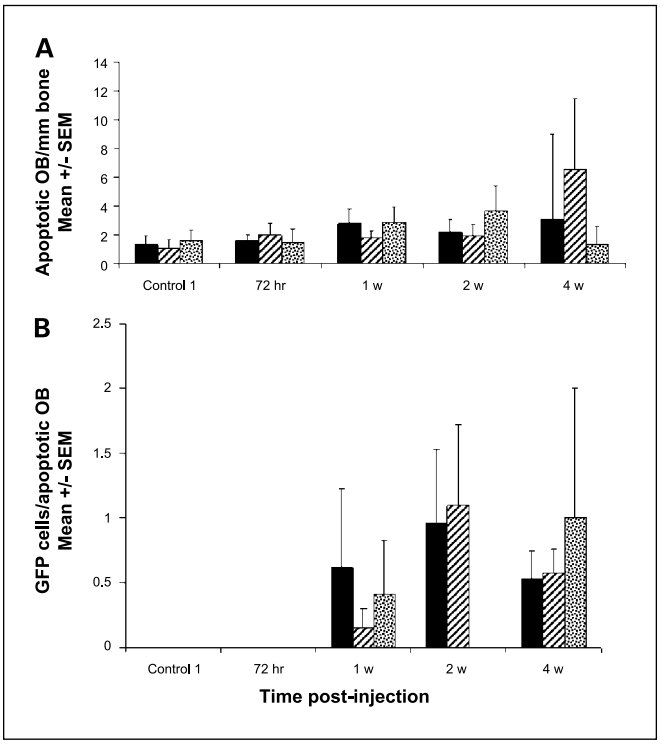

Fig. 4. The presence of metastatic breast cancer cells in close proximity to apoptotic osteoblasts increased with time following inoculation of MDA-435^{GFP}. *A,* apoptotic osteoblasts, detected by TUNEL, were counted in proximal and distal ends of paraffin sections of femur at times following tumor cell inoculation. *B,* number of MDA-435^{GFP} cells within a 50 μm radius of each apoptotic osteoblast. Averages from three femurs per time period. Proximal femur (*hatched columns*), distal femur (*stippled columns*), average over femur (*solid columns*). Apoptotic osteoblasts in the diaphyses were extremely rare.

vasculature (reviewed in ref. 37), anatomic and physiologic mechanisms are also likely to be important factors. Approximately 90% of the blood flow goes to the metaphyseal regions whereas a smaller fraction is found in the diaphyses (reviewed in ref. 38). Additionally, blood flow in the diaphysis is still largely vessel-based, whereas in the metaphyses, it is more sinusoidal. In the sinusoids, the rate of blood flow is <10% of that found in capillaries or other vessels (reviewed in ref. 37). Because of the sluggish blood flow, weaker adhesion molecules would not be subject to negative selection as when cells experience stronger sheer forces. However, arrest is not the only variable involved. The relatively rare cells initially seeding the diaphysis fail to remain there for prolonged periods. It is also possible that cancer cells follow a gradient of growth factors or cytokines. We have preliminary evidence[7] that several cytokines are found at much greater concentrations in the metaphysis compared with the diaphysis. The limitations of the present study cannot discriminate between loss of tumor cells to immune killing, apoptosis, sheer forces, etc., versus migration of tumor cells from the diaphysis to the metaphysis.

The earliest arriving tumor cells were mostly located in close proximity to osteoblasts and the bone-lining cells (Fig. 1B). In general, although the animal-to-animal variability was considerable, the majority of cells tended to be in the endosteal marrow, rather than in central marrow (Fig. 5G), suggesting that traversal from the sinusoids to trabecular space occurs relatively rapidly. This pattern is similar to that reported for hematopoietic precursors in bone marrow (29). Regardless of intra-osseous location, the trend was for tumor

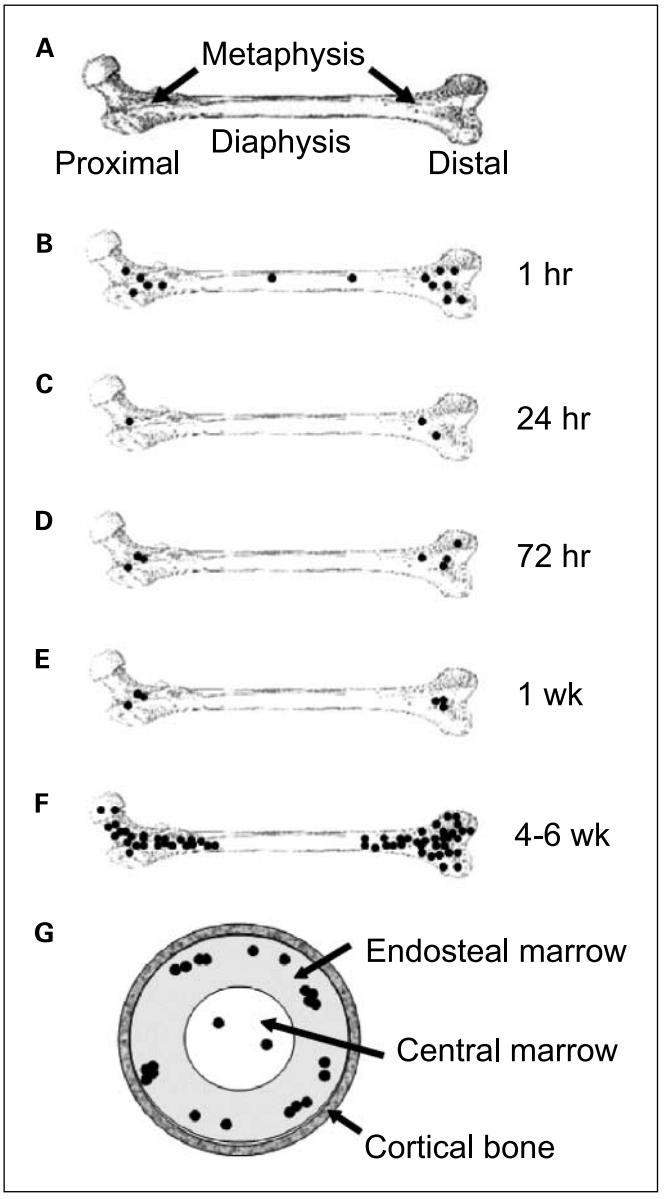

Fig. 5. Schematic diagram depicting colonization of the femur by MDA-435^{GFP} cells. A normal femur is diagramed and labeled for reference (*A*). Single cells (●) arrive in the bone marrow within 1 hour after intracardiac injection (*B*), with a distribution proportionate to the relative blood flow to regions of the bone. Most cells arresting in the bone are cleared within 24 hours (*C*). Of those remaining, the vast majority are still single cells but all are located in the metaphyses. A fraction of the surviving cells begin to proliferate by 72 hours (*D*) with little change in the number of foci, or size of tumor cell clusters, at 1 week postinoculation (*E*). The lesions progressively grow in size so that by 4 to 6 weeks, the mass of the metastases is large and the number of independently seeded cells are indiscernible because the foci have coalesced. Despite not seeding and remaining in the diaphyses, metastases extends into the bone shaft as the lesions grow (*F*). Flushing of bone marrow in established metastases as depicted in Fig. 2, revealed that most of the tumor cells are found in endosteal marrow (~90%) or in the central marrow (~10%), but never in the cortical bone of the diaphysis, as depicted in a cross-sectional view (*G*).

[7] A.M. Mastro, K.M. Bussard, and L. Shuman, unpublished observations.

cell numbers to decline during the first 72 hours after arrival (Fig. 5C and D).

It was somewhat surprising to find that most tumor cells had not begun to proliferate within 72 hours because proliferation typically begins much sooner (i.e., <48 hours) in lungs and orthotopic sites.[8] The period of quiescence or dormancy could be relevant because recent clinical studies have shown that 20% to 100% of women with breast cancer have evidence of disseminated tumor cells in the skeleton (35, 39, 40). Disseminated occult tumor cells within bone are thought to be in a sanctuary from which tertiary metastases could form and are thought to be responsible for late (sometimes months or years) recurrences. Based on abundant evidence from multiple experimental models, the fraction of disseminated cells progressing to overt metastasis is small. However, the presence of disseminated cells predicts poor prognosis in many tumor types, emphasizing that their presence at non-orthotopic sites should not be ignored (39, 40).

What triggers the conversion from dormant to proliferative cells remains unknown and is the subject of intense current investigation. The data presented here do not clarify the mechanistic issue, except to note that there is a substantial delay (72 hours) before the breast carcinoma cells begin to divide. Perhaps, during that time, tumor cells are altering the microenvironment. At our limits of detection, we could not tell whether there was balanced division (i.e., one of two of the progeny died or were eliminated) or whether tumor cells were adapting to the bone microenvironment prior to initiating growth. Upon arriving at a secondary site, tumor cells may remain dormant, undergo a limited number of cell divisions, or continue proliferating to form an overt mass. Presumably, the decisions are based on the response to signal(s) from the local microenvironment. There are self-evident cues that the tissue environment controls the development of bone metastasis based on the patterns of metastasis observed—e.g., metaphyseal > diaphyseal; distal > proximal; endosteal marrow > central marrow. The findings support and extend Stephen Paget's Seed and Soil hypothesis, by which he explains the predilection of breast carcinomas to colonize bone over other tissues (41). In short, Paget posited that tumor cells (seeds) were best suited for growth only in certain tissues (soils). The data presented here indicate that the soil may differ even within individual bones. Indeed the patterns of clinical bone metastases show marked preference for proximal and trabecular bone compared with distal or cortical bone (4). Surprisingly, the metastases arising from injection of MDA-435^{GFP} cells showed the opposite pattern—a slight, but consistent, penchant for distal, compared with proximal, femur. The pattern was consistent regardless of the method used to detect tumor cells. Hence, trivial experimental variables cannot explain why, in this model, metastases develops in the distal femur with greater frequency. One possibility invokes anatomic differences between mice and humans. Mice have extremely different gaits and mechanical pressures on their joints. Because tumor cells are generally predisposed to colonize injured tissues, biomechanical stresses on the knees in mice could, in part, explain the difference in arrest and colonization patterns between the species.

Notwithstanding preferential arrest/adhesion and growth in the metaphyses, metastatic breast carcinoma cells could still survive and grow in the diaphyses when the metastatic lesions are large enough. This growth pattern may suggest that tumor cells renovate the bone microenvironment sufficiently to reduce (or eliminate?) negative signals or that they can induce the production of positive factors from local, nontumor cells. Whether neoplastic cells have surpassed a threshold number, or whether some negative influence on tumor cells has been overcome, the incapacity to colonize diaphyses is not absolute.

It is widely accepted that metastatic breast carcinoma cells manipulate the bone microenvironment to induce osteolysis. In particular, tumor cell activation of osteoclasts via the "vicious cycle" of secretion of PTHrP or RANK ligand has been implicated in bone resorption (4, 19, 42). However, we previously hypothesized that the balance of bone deposition and resorption could be altered as well by reducing osteoblast number or differentiation and/or activity (33). *In vitro* coculture of metastatic human breast carcinoma cells or their conditioned medium with human osteoblasts resulted in apoptosis of the osteoblasts (33). The *in vivo* data presented here extend the previous findings by demonstrating that osteoblasts in the regions colonized by MDA-435^{GFP} are also eliminated.

It is possible that changes in the ratio of osteoblasts to osteoclasts in tumor-infiltrated bone tilts the balance in favor of increasing osteoclastic activity, thereby promoting osteolysis. The dramatic decrease in osteoblasts observed by 4 weeks prompted closer examination of osteoblast apoptosis at multiple times using TUNEL. The number of apoptotic osteoblasts progressively increased until later times, perhaps due to the already decreased number of osteoblasts. Interestingly, at earlier times (<4 weeks) at least one tumor cell was in direct contact (≤50 μm) with each TUNEL-positive osteoblast (Figs. 3E and 4B). Although this finding does not prove that tumor cells directly induce apoptosis, the data are consistent with this hypothesis. We also found with *in vitro* studies that breast cancer cell–conditioned medium prevented osteoblasts from differentiating as evidenced by lack of production of alkaline phosphatase, osteocalcin, and bone siaoloprotein (34). In this current study, the lack of alkaline phosphatase activity (Fig. 3H and I) may be due, in part, to failure of preosteoblasts to differentiate as well as apoptosis of mature osteoblasts. In either case, the outcome is the same, lack of functional osteoblasts.

Ours is the first *in vivo* evidence that tumor cells influence not only osteoclasts, as widely believed and showed, but also osteoblasts. The findings may explain, in part, the failure of bisphosphonate-treated patients to repair osteolytic bone lesions (43)—i.e., if there are no osteoblasts to reconstitute the bone, the lesions will remain.

It was surprising that osteoclast numbers were dramatically reduced in late-stage bone metastasis. Perhaps it should not have been because Orr, Mundy, and colleagues previously described that tumor cells themselves (i.e., in the absence of osteoclasts) could resorb bone (44, 45). The published data, although somewhat controversial, and the evidence presented here leave open the possibility that further progression of osteoclast-initiated osteolysis is possible. Furthermore, previous publications have shown significantly diminished osteoblast and osteoclast numbers in late stage breast carcinoma

[8] Unpublished observations.

metastasis to bone (46–48). Based on heterogeneity among tumors for multiple variables, molecular mechanisms of bone metastasis may vary while yielding the same end point, osteolysis.

A potential criticism of the reported work is that the findings are based on a single cell line. Given the heterogeneity of tumors and the redundant mechanisms from which each can choose to accomplish a given task, we are careful not to overgeneralize. Nonetheless, most key observations reported here have been replicated in the MDA-MB-231 breast carcinoma model of bone metastasis. MDA-MB-231 cells form osteolytic lesions with similar distribution as those found in MDA-MB-435. With expansion of bone lesions, osteoblast numbers decrease in MDA-MB-231 as well.[9] Assuming that the essential elements of osteolytic metastasis are observed in multiple breast carcinoma models, the findings reported here have significant implications with regard to control of bone metastasis in the clinic.

Foremost, the osteoblast is key. Whereas tumor cells could initiate growth prior to osteolysis, one of the earliest observed changes is the elimination of bone-forming cells. Even if bone resorption is controlled exogenously (i.e., by treatment with bisphosphamates), repair of defects is not possible. Because the structural integrity of the skeleton is critical to survival and quality of life, comprehensive treatment needs to restore bone matrix as well as limit osteolysis. By studying the trafficking of tumor cells within the bone and the effect of their presence on normal bone physiology, insights regarding how to improve control of bone metastasis will be forthcoming. Since the submission of this article, a report (49) describing a role for Dickkopf-1 in a Wnt-mediated pathway in prostate cancer cell osteoblastic lesions was published. Whether breast cancer–mediated osteolysis via impairment of osteoblast function is regulated by Dickkopf-1 or other components of the Wnt signaling pathway remains to be determined.

[9] P.A. Phadke and D.R. Welch, unpublished observations.

Acknowledgments

We are indebted to the superb technical assistance from Virginia R. Gilman as well as Patti Lott at the University of Alabama at Birmingham, Center for Metabolic Bone Disease Histomorphometry Core Facility, the University of Alabama at Birmingham Breast Specialized Programs of Research Excellence Tissue Core Facility, Deborah Grove and the Penn State Nucleic Acid Core Facility, and the Penn State Electron Microscopy and Histology Core Facility. We appreciate the critical reading of the manuscript and helpful suggestions from Dr. Tom Clemens.

References

1. Body JJ. Metastatic bone disease: clinical and therapeutic aspects. Bone 1992;13:S57–62.
2. Coleman RE. Skeletal complications of malignancy. Cancer 1997;80:1588–94.
3. Coleman RE, Rubens RD. The clinical course of bone metastases from breast cancer. Br J Cancer 1987;55:61–6.
4. Mundy GR. Metastasis: metastasis to bone: causes, consequences and therapeutic opportunities. Nat Rev Cancer 2002;2:584–93.
5. Lelekakis M, Moseley JM, Martin TJ, et al. A novel orthotopic model of breast cancer metastasis to bone. Clin Exp Metastasis 1999;17:163–70.
6. Chirgwin JM, Guise TA. Molecular mechanisms of tumor-bone interactions in osteolytic metastases. Crit Rev Eukaryot Gene Expr 2000;12:159–78.
7. Guise TA. Parathyroid hormone-related protein and bone metastases. Cancer 1997;80:1572–80.
8. Yoneda T, Sasaki A, Mundy GR. Osteolytic bone metastasis in breast cancer. Breast Cancer Res Treat 1994;32:73–84.
9. Averbuch SD. New bisphosphonates in the treatment of bone metastases. Cancer 1993;72:3443–52.
10. Wetterwald A, van der Pluijm G, Que I, et al. Optical imaging of cancer metastasis to bone marrow—a mouse model of minimal residual disease. Am J Pathol 2002;160:1143–53.
11. Holleran JL, Miller CJ, Culp LA. Tracking micrometastasis to multiple organs with *lacZ*-tagged CWR22R prostate carcinoma cells. J Histochem Cytochem 2000;48:643–51.
12. Amhlaoibh RN, Hoegh-Andersen P, Brünner N, et al. Measurement of tumor load and distribution in a model of cancer-induced osteolysis: a necessary precaution when testing novel anti-resorptive therapies. Clin Exp Metastasis 2004;21:65–74.
13. Sung V, Cattell DA, Bueno JM, et al. Human breast cancer cell metastasis to long bone and soft organs of nude mice: a quantitative assay. Clin Exp Metastasis 1997;15:173–83.
14. Murphy BO, Joshi S, Kessinger A, Reed E, Sharp JG. A murine model of bone marrow micrometastasis in breast cancer. Clin Exp Metastasis 2002;19:561–9.
15. Harms JF, Welch DR. MDA-MB-435 human breast carcinoma metastasis to bone. Clin Exp Metastasis 2003;20:327–34.
16. Yang M, Baranov E, Jiang P, et al. Whole-body optical imaging of green fluorescent protein-expressing tumors and metastases. Proc Natl Acad Sci U S A 2000;97:1206–11.
17. Manolagas SC. Birth and death of bone cells: basic regulatory mechanisms and implications for the pathogenesis and treatment of osteoporosis. Endocr Rev 2000;21:115–37.
18. Parfitt AM. Osteonal and hemi-osteonal remodeling: the spatial and temporal framework for signal traffic in adult human bone. J Cell Biochem 1994;55:273–86.
19. Roodman GD. Mechanisms of disease: mechanisms of bone metastasis. N Engl J Med 2004;350:1655–64.
20. Van Tine BA, Kappes JC, Banerjee NS, et al. Clonal selection for transcriptionally active viral oncogenes during progression to cancer. J Virol 2004;78:11172–86.
21. Chen W, Wu X, Levasseur DN, et al. Lentiviral vector transduction of hematopoietic stem cells that mediate long-term reconstitution of lethally irradiated mice. Stem Cells 2000;18:352–9.
22. Sellappan S, Grijalva R, Zhou XY, et al. Lineage infidelity of MDA-MB-435 cells: expression of melanocyte proteins in a breast cancer cell line. Cancer Res 2004;64:3479–85.
23. Harms JF, Welch DR, Samant RS, et al. A small molecule antagonist of the α-v, β-3 integrin suppresses MDA-MB-435 skeletal metastasis. Clin Exp Metastasis 2004;21:119–28.
24. Parfitt AM. Bone histomorphometry: proposed system for standardization of nomenclature, symbols, and units. Calcif Tissue Int 1988;42:284–6.
25. Parfitt AM, Drezner MK, Glorieux FH, et al. Bone histomorphometry: standardization of nomenclature, symbols, and units. Report of the ASBMR Histomorphometry Nomenclature Committee. J Bone Miner Res 1987;2:595–610.
26. Miao D, Scutt A. Histochemical localization of alkaline phosphatase activity in decalcified bone and cartilage. J Histochem Cytochem 2002;50:333–40.
27. Harms JF, Budgeon LR, Christensen ND, Welch DR. Maintaining green fluorescent protein tissue fluorescence through bone decalcification and long-term storage. Biotechniques 2002;33:1197–200.
28. Jewell J, Mastro AM. Using terminal deoxynucleotidy transferase (TDT) enzyme to detect TUNEL-positive, GFP-expressing apoptotic cells. Appl Cell Notes 2002;3:13–4.
29. Mason TM, Lord BI, Hendry JH. The development of spatial distributions of CFU-S and *in vitro* CFC in femora of mice of different ages. Br J Haematol 1989;73:455–61.
30. Mager DL, Medstrand P. Retroviral repeat sequences. In: Anonymous encyclopedia of the human genome. London: Macmillan Publishers Ltd., Nature Publishing Group; 2003. p. 1–7.
31. Goldberg SF, Harms JF, Quon K, Welch DR. Metastasis-suppressed C8161 melanoma cells arrest in lung but fail to proliferate. Clin Exp Metastasis 1999;17:601–7.
32. Fidler IJ. Metastasis: quantitative analysis of distribution and fate of tumor emboli labeled with ^{125}I-5-iodo-2′-deoxyuridine. J Natl Cancer Inst 1970;45:773–82.
33. Mastro AM, Gay CV, Welch DR, et al. Breast cancer cells induce osteoblast apoptosis: a possible contributor to bone degradation. J Cell Biochem 2004;91:265–76.
34. Mercer RR, Miyasaka C, Mastro AM. Metastatic breast cancer cells suppress osteoblast adhesion and differentiation. Clin Exp Metastasis 2004;21:427–35.
35. Masuda TA, Kataoka A, Ohno S, et al. Detection of occult cancer cells in peripheral blood and bone marrow by quantitative RT-PCR assay for cytokeratin-7 in breast cancer patients. Int J Oncol 2005;26:721–30.
36. Lipton A. Management of bone metastases in breast cancer. Curr Treat Options Oncol 2005;6:161–71.
37. Welch DR, Harms JF, Mastro AM, Gay CV. Breast cancer metastasis to bone: evolving models and research challenges. J Musculoskelet Neuronal Interact 2003;3:30–8.
38. Gross TS, Clemens TL. Vascular control of bone remodeling. In: Anonymous advances in organ biology. JAI Press Inc.; 1998. p. 138–60.
39. Pantel K, Woelfle U. Micrometastasis in breast cancer and other solid tumors. J Biol Regul Homeost Agent 2004;18:120–5.
40. Pantel K, Brakenhoff RH. Dissecting the metastatic cascade. Nat Rev Cancer 2004;4:448–56.
41. Paget S. The distribution of secondary growths in cancer of the breast. Lancet 1889;1:571–3.
42. Lynch CC, Hikosaka A, Acuff HB, et al. MMP-7

promotes prostate cancer-induced osteolysis via the solubilization of RANKL. Cancer Cell 2005;7: 485–96.

43. Lipton A, Theriault RL, Hortobagyi GN, et al. Pamidronate prevents skeletal complications and is effective palliative treatment in women with breast carcinoma and osteolytic bone metastases—long term follow-up of two randomized, placebo-controlled trials. Cancer 2000;88:1082–90.

44. Eilon G, Mundy GR. Direct resorption of bone by human breast cancer cells *in vitro*. Nature 1978;276: 726–8.

45. Sanchez-Sweatman OH, Orr FW, Singh G. Human metastatic prostate PC3 cell lines degrade bone using matrix metalloproteinases. Invasion Metastasis 1998; 18:297–305.

46. Stewart AF, Vignery A, Silverglate A, et al. Quantitative bone histomorphometry in humoral hypercalcemia of malignancy: uncoupling of bone cell activity. J Clin Endocrinol Metab 1982;55:219–27.

47. Sanchez Y, Bachant J, Wang H, et al. Control of the DNA damage checkpoint by Chk1 and Rad53 protein kinases through distinct mechanisms. Science 1999; 286:1166–71.

48. Mundy CR, Altman AJ, Gondek MD, Bandelin JG. Direct resorption of bone by human monocytes. Science 1977;196:1109–11.

49. Hall CL, Bafico A, Dai J, Aaronson SA, Keller ET. Prostate cancer cells promote osteoblastic bone metastases through Wnts. Cancer Res 2005;65:7554–60.